MIMO Performance of Realistic UE Antennas in LTE Scenarios at 750 MHz

Fredrik Athley, Anders Derneryd, *Senior Member, IEEE*, Jonas Fridén, Lars Manholm, and Anders Stjernman

***Abstract*—Multiple-input–multiple-output (MIMO) is a technique to achieve high data rates in mobile communication networks. Simulations are performed at both the antenna level and Long-Term Evolution (LTE) system level to assess the performance of realistic handheld devices with dual antennas at 750 MHz. It is shown that MIMO works very well and gives substantial performance gain in user devices with a quarter-wavelength antenna separation.**

***Index Terms*—Long-Term Evolucation (LTE), multiple-input–multiple-output (MIMO), simulations, user equipment (UE) antennas.**

I. Introduction

NEW GENERATIONS of high-data-rate services integrated in mobile communication networks as well as the broad range of available frequency bands have increased the requirements on antennas that are used in mobile devices. These requirements include high efficiency, low antenna branch signal correlation, and capability to handle multifrequency bands. This poses significant challenges for antenna designers of user equipment (UE) when integrating more antenna functions within a limited volume such as a handheld device.

In this letter, measured antenna radiation patterns of a number of multiantenna UEs intended for the Long-Term Evolution (LTE) band 13 are used to evaluate realistic antenna implementations. Novel contributions of the letter are the following.

1) Multiple-input–multiple-output (MIMO) performance for antenna implementations in realistic handhelds at 750 MHz is evaluated.
2) Antenna metrics for MIMO system performance are identified.
3) MIMO performance of realistic handhelds and ideal dipoles are compared.

II. Simulation Models

A. Antenna Models

System simulators usually employ ideal models of the UE antennas. Typical assumptions are the following:

- omnidirectional radiation patterns;
- unit gain for all antenna ports;
- vertical polarization;
- half a wavelength antenna separation;
- no antenna interaction.

A real UE antenna realization does not fulfill these assumptions. Typical properties of real multiantennas in a UE are the following:

- mutual coupling;
- polarization angular variation;
- nonorthogonal radiation patterns;
- losses that reduce the gain of the antenna;
- dissimilar radiation patterns at different antenna ports.

In this letter, we use measured embedded (the other antennas perfectly matched) antenna radiation patterns of four different handheld dual-antenna smartphone devices and a reference case with ideal orthogonal dipoles.

B. Channel Models

The simplest model of the power spectrum of incident rays is the uniform Clarke's scenario where all scatterers are in the horizontal plane [1]. This far-field model in this letter is extended to a uniform full-sphere model where waves are uniformly distributed over the entire sphere.

The spatial channel model (SCM) developed within the 3GPP standardization body in order to evaluate MIMO performance of mobile systems in predefined environments is also employed [2], [3]. The model simulates a polarized bidirectional propagation channel. The generic channel model is a set of rays described by geometrical and propagation features such as delay, direction of departure and arrival at the base station and the user device, and a polarization matrix. Polarization needs to be included in the channel modeling when evaluating the impact of using realistic antennas.

The SCM currently defines three environments, namely suburban macro, urban macro, and urban micro. There is a fixed number of six paths (scatterers) in every environment that contains 20 spatially separated subpaths each. The mobile channel is modeled as a set of propagation paths where signal power, delay, and angular properties for both sides of the link are modeled as random variables.

For a normalized far-field radiation pattern $\vec{F}_n(\Omega)$, the signal received on the antenna port n reads [4, Eq. (18)]

$$H_{nm} = \frac{1}{\sqrt{4\pi}} \iint_{4\pi} \vec{F}_n(\Omega) \cdot \vec{h}_m(\Omega) d\Omega \tag{1}$$

where $\vec{h}_m(\Omega)$ is the normalized incident field produced from transmit antenna m. The thus calculated channel response matrix is then used to calculate, e.g., the channel capacity.

Manuscript received July 13, 2011; revised August 31, 2011, September 28, 2011; accepted November 02, 2011. Date of publication November 23, 2011; date of current version December 12, 2011.

The authors are with Ericsson AB, Gothenburg 417 56, Sweden (e-mail: anders.derneryd@ericsson.com).

Color versions of one or more of the figures in this letter are available online at http://ieeexplore.ieee.org.

Digital Object Identifier 10.1109/LAWP.2011.2177237

Fig. 1. Illustration of antenna location in dual-antenna devices (A and B) in a medium-size smartphone form factor.

The incident field is discretized in a number of plane waves, or rays, with the spatial distribution taken from the three environments described in 3GPP SCM [2], [3].

C. System Scenarios

In the link-level performance evaluations, the three environments specified in 3GPP SCM are used. In the system-level evaluations, two different system scenarios are used: one with high and one with low intercell interference, respectively. These are based on the 3GPP cases 1 and 3 as specified in [5]. The high-interference scenario is based on 3GPP case 1 with on average five UEs/cell, and the low-interference scenario is based on 3GPP case 3 with on average 0.1 UEs/cell. The network consists of 19 three-sector sites placed on a hexagonal grid with 500 m intersite distance for case 1 and 1732 m for case 3. In these scenarios, the urban macro channel environment in 3GPP SCM is used.

III. User Devices

A number of dual-antenna UEs have been designed and manufactured by Sony Ericsson Mobile Communications in Lund, Sweden. These devices have two internal antennas that are connected via cables in order to be able to record the embedded radiation patterns. Two devices have the outer dimensions of a medium-size smartphone, $115 \times 65 \times 12$ mm^3 ($0.29\lambda \times 0.16\lambda \times 0.03\lambda$ at 750 MHz). The first one has a main monopole antenna (6% bandwidth at 10-dB return loss) located at the bottom edge of the device, while an equally aligned monopole diversity antenna (6% bandwidth) is placed at the top edge as shown to the left in Fig. 1. The second device, shown in the right photograph in Fig. 1, has a notch diversity antenna (3% bandwidth) orthogonally placed along the side edge. The designs are intentionally chosen such that the antenna pattern correlations are in the high and low midrange, respectively.

Another set of devices has the outer dimensions of a larger smartphone, $150 \times 73 \times 22$ mm^3 ($0.37\lambda \times 0.18\lambda \times 0.06\lambda$ at 750 MHz). The main monopole antenna (27% bandwidth) is located at the top edge of device 1, while the planar inverted-F antenna (PIFA) diversity antenna (3% bandwidth) is placed orthogonally at the lower edge, as illustrated to the left in Fig. 2. The other device has two colocated loop antennas (5% and 7% bandwidth, respectively) as large as the PIFA in the first device and positioned at the bottom edge (right photograph in Fig. 2).

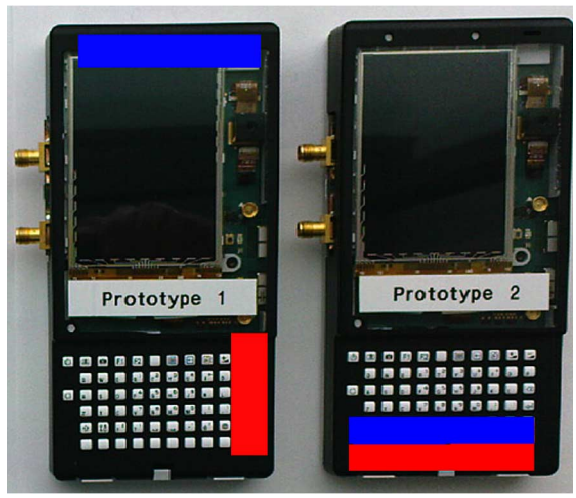

Fig. 2. Illustration of antenna location in dual-antenna devices (1 and 2) with dimensions of a larger smartphone.

The first device is designed to have a low antenna pattern correlation, while the second device is intentionally designed for very high correlation. The antenna separation in all devices is less than a quarter-wavelength.

IV. Antenna Characteristics

Antenna parameters are evaluated at 750 MHz. Samples of the measured total power (sum of θ and ϕ components of the far field) radiation patterns for device 1 in free space are displayed in Fig. 3. The device is placed in a browse mode, i.e., tilted 45° backward.

The complex correlation properties of the radiation patterns are studied to further examine the radiation characteristics. Another way of looking at radiation characteristics is to study correlation due to magnitude only (constant phase at both antenna ports) and phase only (equal magnitude of θ and ϕ components at both antenna ports). These analyses show which diversity aspect is more critical in reducing correlation.

A few results of the antenna characteristics at 750 MHz are summarized in Table I, where a spherical uniform spectrum of the incident field is assumed. Mean efficiency is calculated as the average efficiency of the two antennas, and pattern correlation is defined in [4, Eq. (29)]. It is observed that the magnitude-only radiation patterns are highly correlated in all four cases, while the phase-only patterns differentiate the devices, indicating that mainly spatial separation reduces correlation. Orthogonal placement of the antennas further distinguishes device B from device A.

V. MIMO Performance

The channel capacity of a MIMO antenna system is calculated according to [6] using embedded gain normalized radiation patterns as the only antenna parameter. The theoretical values using two totally uncorrelated lossless dipoles are used as a reference setup. Different power spectra of the incident field are assumed such as spherical uniform, urban macro, suburban macro, and urban micro. The relative 2×2 channel capacities of the devices assuming water filling at a signal-to-noise ratio (SNR) level of 20 dB are summarized in Table II.

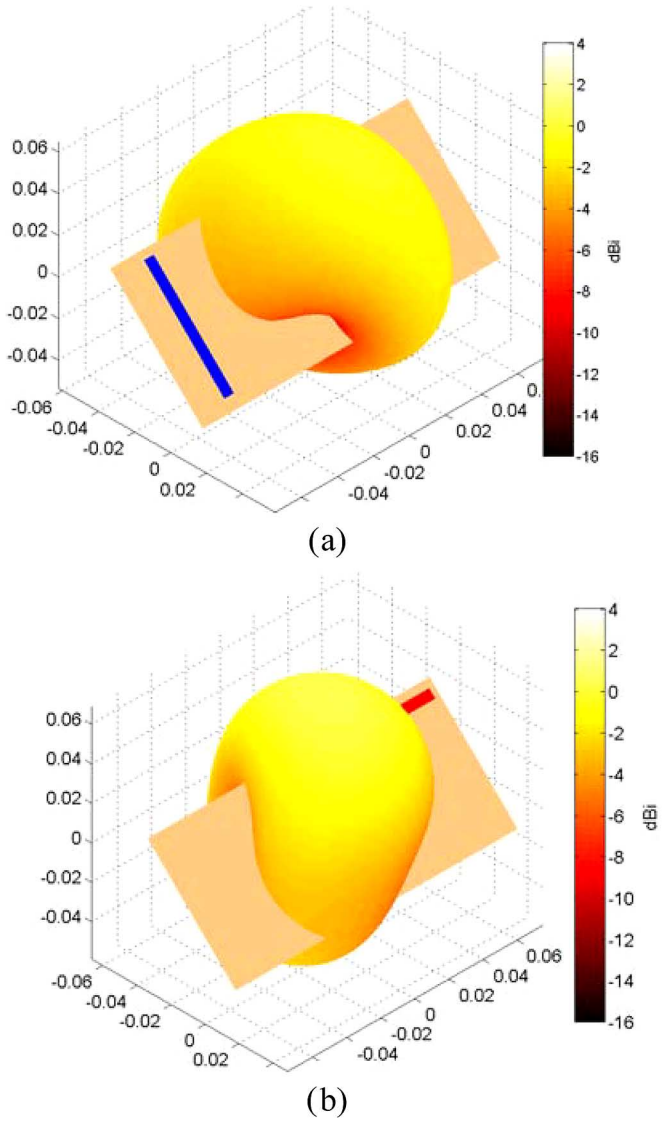

Fig. 3. Measured embedded total power radiation patterns of device 1 tilted 45° backwards at 750 MHz. (a) Main antenna. (b) Diversity antenna.

TABLE I
ANTENNA CHARACTERISTICS OF THE EVALUATED DEVICES

Parameter \ Device	A	B	1	2
Main antenna efficiency (dB)	-5.4	-3.6	-3.3	-4.9
Diversity antenna efficiency (dB)	-4.3	-4.6	-2.5	-5.6
Mean efficiency (dB)	-4.8	-4.1	-2.9	-5.2
Magnitude only correlation	0.94	0.95	0.96	1.00
Phase only correlation	0.48	0.32	0.02	0.92
Magnitude of complex correlation	0.71	0.42	0.24	0.97
MIMO efficiency (dB)	-6.4	-4.6	-3.0	-11.2

A metric that relates the MIMO performance of real antennas to ideal antennas is the MIMO efficiency [7] also known as the multiplexing efficiency [8] and related to ellipticity statistics [9]. MIMO efficiency is a measure of the additional SNR

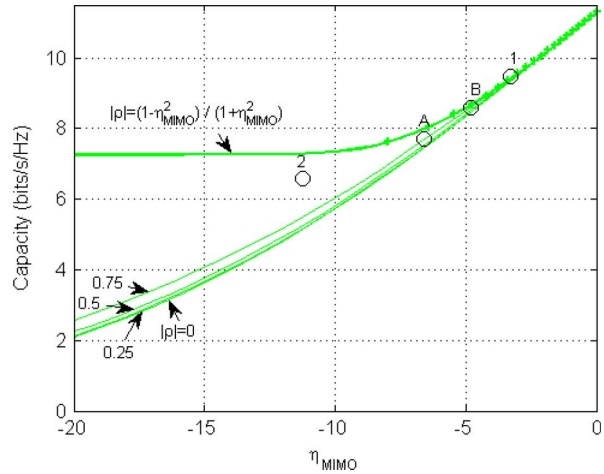

Fig. 4. Channel capacity at 20-dB SNR as a function of MIMO efficiency assuming a spherical uniform power spectrum of the incident field and with the magnitude of the complex correlation as a parameter.

TABLE II
RELATIVE CHANNEL CAPACITY OF THE DEVICES COMPARED TO TWO ORTHOGONAL AND LOSSLESS DIPOLES IN PERCENT AT SNR 20 dB IN FOUR DIFFERENT CHANNELS

Channel \ Device	A	B	1	2
Spherical uniform	68	76	84	58
SCM urban macro	77	83	89	72
SCM suburban macro	78	83	89	73
SCM urban micro	72	80	87	64

required for a real antenna to achieve the same capacity as an ideal antenna in an independent and identically distributed fading channel. In a 2×2 MIMO antenna application, the MIMO efficiency at high SNR is given by [8]

$$\eta_{\text{MIMO}} = \sqrt{\eta_1 \eta_2 (1 - |\rho|^2)} \tag{2}$$

where η_1 and η_2 are the antenna efficiency of antenna 1 and 2, respectively, and ρ is the antenna pattern complex correlation. Hence, MIMO efficiency is determined by the complex correlation and the geometric mean of the antenna efficiencies. It is a simple and intuitive metric since the contributions due to efficiency and correlation are separated when evaluating the effectiveness of MIMO terminal antennas.

The MIMO efficiencies for the four devices are presented in Table I. It is noted that the MIMO efficiency is partly due to the antenna mean efficiencies, which vary between -2.9 and -5.2 dB, and partly due to the correlation. For example, devices A and 2 have only 0.4 dB difference in mean antenna efficiencies, but 4.8 dB difference in MIMO efficiencies, mainly due to much higher correlation in device 2. According to Table I, the correlation contributes to a 1.6-dB reduction in device A, while in device 2 the correlation is responsible for a 6-dB loss in MIMO efficiency. In device 1, the correlation is due to only a 0.1-dB decrease. The 2×2 channel capacities at 20-dB SNR are displayed in Fig. 4 as a function of the MIMO efficiency and correlation in a spherical uniform power spectrum of the incident field. The performances of the four devices are marked with a ring.

TABLE III
2×2 MIMO THROUGHPUT OF DEVICES IN THE SCM URBAN MACRO ENVIRONMENT RELATIVE TO TWO IDEAL DIPOLES IN PERCENT

Parameter \ Device		A	B	1	2
3GPP case 1, high load	System	88	96	99	71
	Cell-edge	78	93	96	67
	Peak	92	97	100	72
3GPP case 3, low load	System	75	83	90	64
	Cell-edge	59	67	77	50
	Peak	81	90	95	55

Furthermore, downlink system simulations are performed with a fairly detailed multicell LTE radio network simulator, which includes the 3GPP SCM and models of, e.g., adaptive coding and modulation, UE mobility, and delays in channel quality reports. The performance is assessed using system and user throughput. Throughput is defined as the total number of correctly received bits divided by the total simulation time. The 3GPP cases 1 and 3 are studied with the SCM urban macro environment. Table III shows the system, cell-edge (5%), and peak (95%) throughput for the antenna devices relative to the ideal dipoles. All throughput values are normalized so that 100% corresponds to the throughput obtained when using the ideal reference antenna. The base station has a dual-polarized ($\pm 45^{\circ}$) antenna, which radiation patterns are modeled as in [10]. The results in Table III are based on the same radio network simulator, scenarios, and simulation methodology as reported in [11].

From Table III, it is clear that the devices with well-designed antennas achieve MIMO performance on par with the ideal reference antennas, particularly in the scenario with high intercell interference (3GPP case 1). If the devices are ranked according to performance, it can be seen that the antenna characteristics in Table I, the link-level results in Table II, and the system-level results in Table III give consistent rankings.

VI. CONCLUSION

It is seen from the simulations on realistic dual-antenna devices at 750 MHz that substantial MIMO performance is achieved relative to ideal reference dipoles. Actually, the best one of the handhelds performs similarly to the reference case. In scenarios with low load, MIMO performance at cell edge is reduced to about 80% compared to the ideal case, but in a highly loaded scenario, MIMO performance is equally as good as the reference antenna setup.

Additional support for the effectiveness of MIMO techniques at 750 MHz with handheld devices has also recently been published in [12]. Herein, it is demonstrated in field trials in a pre-commercial LTE network that a well-designed antenna gives similar MIMO performance as a reference antenna design that has less stringent restrictions on physical size.

ACKNOWLEDGMENT

The authors wish to thank Sony Ericsson Mobile Communications AB, Lund, Sweden, for providing measured radiation patterns of the evaluated devices.

REFERENCES

[1] R. H. Clarke, "A statistical theory of mobile-radio reception," *Bell Syst. Tech. J.*, vol. 47, pp. 957–1000, Jul.–Aug. 1968.

[2] G. Calcev, D. Chizhik, B. Göransson, S. Howard, H. Huang, A. Kogiantis, A. F. Molisch, A. L. Moustakas, D. Reed, and H. Xu, "A wideband spatial channel model for system-wide simulations," *IEEE Trans. Veh. Technol.*, vol. 56, no. 2, pp. 389–403, Mar. 2007.

[3] 3rd Generation Partnership Project (3GPP), "Spatial channel model for multiple input multiple output (MIMO) simulations," TR 25.996 v 10.0.0, 2011.

[4] R. G. Vaughan and J. B. Andersen, "Antenna diversity in mobile communications," *IEEE Trans. Veh. Technol.*, vol. VT-36, no. 4, pp. 149–172, Nov. 1987.

[5] 3rd Generation Partnership Project (3GPP), "Physical layer aspects for evolved universal terrestrial radio access (UTRA)," TR 25.814 v 7.1.0, 2006.

[6] G. J. Foschini and M. J. Gans, "On limits of wireless communications in a fading environment when using multiple antennas," *Wireless Pers. Commun.*, vol. 6, no. 3, pp. 311–335, Mar. 1998.

[7] A. Derneryd, A. Stjernman, H. Strandberg, and B. Wästberg, "Multi-objective optimization of MIMO antennas for dual-band user devices," in *IEEE Antennas Propag. Int. Symp. Dig.*, Spokane, WA, Jul. 2011, pp. 2449–2452.

[8] R. Tian, B. K. Lau, and Z. Ying, "Multiplexing efficiency of MIMO antennas," *IEEE Antennas Wireless Propag. Lett.*, vol. 10, pp. 183–186, 2011.

[9] J. Salo, P. Suvikunnas, H. M. El-Sallabi, and P. Vainikainen, "Ellipticity statistic as measure of MIMO multipath richness," *Electron. Lett.*, vol. 42, no. 3, pp. 160–162, Feb. 2006.

[10] F. Athley and M. N. Johansson, "Impact of electrical and mechanical antenna tilt on LTE downlink system performance," in *Proc. 71st IEEE VTC–Spring*, Taipei, Taiwan, May 2010.

[11] F. Athley, L. Manholm, J. Fridén, and A. Stjernman, "Practical multi-antenna terminals in LTE system performance simulations," in *Proc. 30th URSI Gen. Assembly Sci. Symp.*, Istanbul, Turkey, Aug. 2011.

[12] B. Hagerman, K. Werner, and J. Tang, "MIMO performance at 700 MHz: Field trials of LTE with handheld UE," in *Proc. 74th IEEE VTC–Fall*, San Francisco, CA, Sep. 2011.